Influence of severe thermal preconditioning on the bond between carbon FRCM and masonry substrate: Effect of textile pre-impregnation

Veronica Bertolli [a], Cesare Signorini [b,c], Andrea Nobili [b], Tommaso D'Antino [a,*]

[a] Department of Architecture, Built Environment and Construction Engineering, Politecnico di Milano, Piazza Leonardo da Vinci, 32, 20133 Milan, Italy
[b] Department of Engineering "Enzo Ferrari", University of Modena and Reggio Emilia, 41125 Modena, Italy
[c] Institute of Construction Materials, TU Dresden, 01187 Dresden, Germany

A R T I C L E   I N F O

A B S T R A C T

Fabric-reinforced cementitious matrix (FRCM) composites often include polymer-impregnated bundles to improve the exploitation of the textile mechanical properties. However, organic components may degrade when exposed to elevated temperature. In this paper, the bond behavior of a carbon FRCM applied to a masonry substrate and exposed to a thermal preconditioning up to 300 °C for 250 min is investigated. Tensile tests on the textile and flexural and compression tests on the mortar matrix, as well as single-lap direct shear tests of FRCM-masonry joints with bare and impregnated textiles, are performed. Results show that the polymeric impregnation improves the mechanical properties of the FRCM even after thermal preconditioning.

1. Introduction

Externally bonded reinforcements (EBR) realized with composites embedding high-strength textiles and inorganic matrices currently represent a viable option for refurbishing and retrofitting concrete and masonry structures. These composites are usually referred to as fabric-reinforced cementitious matrix (FRCM), textile-reinforced concrete (TRC), or textile-reinforced mortar (TRM). Compared to traditional reinforcement strategies, such as steel and reinforced concrete jacketing, FRCMs impart remarkable mechanical performance, while allowing for minimal impact on the existing structure. Furthermore, FRCMs are characterized by high strength-to-weight ratio and wide flexibility in the application process, which pave the way to highly optimized design.

Recently, the scientific community has devoted great efforts into the development of textile-reinforced EBR [1–4], especially with the goal of enhancing the physical and mechanical characteristics of the interface between the textile and surrounding matrix [5,6]. Typically, bundle coatings and impregnations are employed to improve chemical affinity between the textile and the inorganic matrix and to guarantee thorough fiber impregnation within each bundle. Indeed, bare/dry textile bundles usually consist of several thousands of tightly packed filaments, whose mutual spacing is incompatible with inorganic matrix impregnation. In fact, this spacing is of the order of a few microns and cannot accommodate the average particle size of common lime and cementitious

mortars. This incompatibility leads to good matrix impregnation of the outer fiber filaments only, i.e., the sleeve filaments, whereas core filaments are not impregnated. This entails for a reduced exploitation of the textile tensile properties, as widely documented in the literature [7–9]. Bundle coating and impregnation represent an effective solution to tackle this issue, and polymer coatings generally provide the best performance [6,10]. Indeed, the liquid polymer phase is able to penetrate the bundle and its hardening reaction promotes the monolithic behavior of the bundle, associated with an even distribution of the external load [11]. Although the mechanical properties and the bond characteristics of FRCM composites have been thoroughly investigated, limited attention has been devoted to assessing their durability, which still represents an open issue. A few studies report significant performance loss after accelerated ageing and weathering, with particular reference to salt-water and alkaline environments [12–16]. Nonetheless, a comprehensive approach to durability that considers the vast range of strengthening materials and matrices currently available in the market is still lacking, and so are common guidelines to be used in the design stage. As notable exceptions, United States (US) [17] and Italian [18] acceptance criteria (AC) for FRCM composites provide specific aging protocols and tensile test methods for assessing the composite long-term behavior. In addition, the European assessment document EAD 340275–00-0104 [19] provides testing and quality control procedures to obtain the European technical approval (ETA) and CE mark for EBR comprising

* Corresponding author.
  E-mail address: tommaso.dantino@polimi.it (T. D'Antino).

inorganic-matrix composites. The United States (US) [17] and Italian [18] AC require the tensile mechanical properties of FRCM to be evaluated also taking into account specific environmental conditions, such as high relative humidity exposure, freeze–thaw cycles, and exposure to alkaline and saline environments. In this spirit, a landscape comparison of textile durability has been recently presented by Signorini and Nobili [20], in the shape of a design matrix of *environmental conversion factors* comparing six different types of textile reinforcement.

Tensile tests to evaluate the composite performance after a thermal conditioning protocol of a specific time duration are also envisaged by the Italian AC [18]. The difference in the load response of specimens tested at ambient temperature with respect to specimens tested under a specific temperature (declared by the manufacturer) should be assessed, and the corresponding degradation should not exceed 15 % for any strain value. The rationale behind this prescription, however, is not completely clear and more investigations on FRCM thermal conditioning are needed to better frame its role.

Broadening the view to encompass the interaction between the strengthening material and the structural element, single-lap direct shear tests is largely employed for the assessment of the bond behavior of FRCM-substrate joints, in accordance with the Italian AC [18] and European EAD [19] for FRCM composites. Also, a distinction can be made between elevated and high temperatures (see e.g., Askouni and Papanicolaou [21]). Elevated temperature usually relates with the effects of solar radiation on external surface of buildings, largely exceeding 50 °C in certain geographical areas [22]. It should be noted that 80 °C is the maximum temperature considered by the Italian building code [23]. Temperatures above 300 °C are defined as high [21] and, along with specific time-dependent temperature histories, could simulate fire events, e.g., localized fires [24–26].

The main objection to the application of polymeric coatings in FRCM composites relates to the adoption of a temperature-sensitive material in an otherwise temperature-resistant system. For this reason, FRCM design guidelines limit to 5 %wt. the amount of polymer that may be introduced into the system [27]. Although the amount of polymeric phase added through bundle coating or impregnation generally lies well below this threshold, the thermal stability of the multiphase system should be carefully assessed. However, only few studies in the literature investigated both the effect of elevated and high temperatures on FRCM composites, especially in the presence of polymeric phases in the system. Donnini et al. [28] investigated the mechanical behavior of carbon FRCM exposed to elevated temperature, through clevis-grip tensile and double-lap shear tests. The exposure temperature ranged from 20 °C to 120 °C and some of the tensile and direct shear tests were conducted at elevated temperature. Both bare and impregnated textiles were considered, the latter consisting of wet coating with epoxy resin and sand to enhance the interlocking/friction with the surrounding cement-based matrix. The main failure mode was debonding of the textile from the matrix, regardless of the presence of the coating. As expected, bare carbon textiles exhibited small mechanical performance losses due to temperature exposure, whereas epoxy-coated specimens suffered from a significant strength drop (61 %) when exposed to and tested at 120 °C. Interestingly, a peak load reduction of as little as 7 % was observed for specimens preheated to 120 °C for 60 min and tested at room temperature. Results from Messori et al. [29] set spotlight on the coating composition, which deeply affects the thermal stability of the FRCM. Surprisingly, epoxy coatings including aromatic rings, despite their intrinsic brittleness, showed a significant post-curing process at temperatures ranging between 100 °C and 150 °C, which increased the bearing capacity of the composite. In fact, differential scanning calorimetry demonstrated that epoxy with aliphatic hardener (diethylenetriamine) could polymerize completely (about 96 %) already at ambient temperature, as opposed to the aromatic counterpart (m-phenylenediamine) whose polymerization rate reached only 67 %. This entailed that further polymerization could take place when m-phenylenediamine was subjected to elevated temperatures, thus mitigating the onset of thermal

degradation. For temperatures up to 250 °C, moderate degradation occurred. In general, available studies are limited to 250 °C, with the significant exception of Rambo et al. [30], who tested basalt textiles coated with polymeric latex and combined with refractory concrete preheated up to 1000 °C. Results are comparable with those of Messori et al. [29] up to 150 °C, while extreme thermal loadings, above 400 °C, led to an abrupt drop in the FRCM response. For other contributions dealing with tensile properties of FRCM within the context of thermal aging, the exhaustive review by Kapsalis et al. [31] can be considered. Only a handful of papers investigated the effect of temperature exposure on the bond performance of a composite applied onto a specific substrate. In Maroudas and Papanicolau [32] and Askouni et al. [21], direct shear tests were carried out to assess the effect of elevated temperature – up to 300 °C – on the bond capacity of alkali resistant (AR) glass textile-reinforced mortar (TRM) applied to a masonry substrate. A very steep heating curve, namely 75 °C/min, was chosen to represent a fire event, although the final target temperature was relatively low. In fact, the temperature range was selected to simulate the effect of hot weather and the usual thermal conditions within a nuclear reactor, set at 175 °C. Upon reaching 300 °C, for each of the bonded length considered, the residual bond capacity decreased by 50 %, and the failure mode progressively shifted from fiber slippage (at 20 °C and 100 °C), to detachment of the composite strip from the substrate or fiber rupture (at 200 °C and 300 °C). These results highlighted the vulnerability of bare glass fibers to elevated and high temperatures, and the need for careful fiber protection. Raoof and Bournas [33] investigated the bond behavior of FRP and FRCM composites at elevated and high temperature, conducting double-lap shear tests at the target temperatures. The beneficial role of inorganic matrices was highlighted with respect to epoxy resins. Indeed, while FRP bond capacity degraded up to 83 % at 150 °C, the FRCM counterpart retained most of its performance up to 400 °C (only 15 % reduction). Ombres [34] performed single-lap direct shear tests of PBO FRCM-concrete joints comprising 1- or 2-layer textiles. For thermal conditioning, a single bonded length equal to 250 mm was selected. Specimens were put into an oven and kept at the target temperatures of 50 °C or 100 °C for 8 h, before being slowly cooled down to room temperature for testing. Failure modes appeared significantly scattered with increasing the temperature, whereby in some cases failure shifted from debonding at the matrix-textile interface associated with fiber slippage to debonding at the matrix-textile interface associated with matrix interlaminar failure or to detachment of the FRCM strip from the substrate. Moreover, conditioning at 100 °C heavily affected the test peak load and stiffness. FRCM systems applied to a masonry substrate were investigated in Ombres et al. [35]. Single-lap direct shear tests after thermal conditioning were performed with basalt, steel, and PBO textiles, at temperatures of 100 °C, 150 °C, and 200 °C. In general, a strong reduction was observed in the peak performance. Basalt exhibited an inconsistent behavior, depending on the specific textile under consideration (-17 % and −51 %). A heavy reduction was also observed for steel and PBO FRCM (-40 %). Elevated temperatures led to a significant embrittlement of the composite, i.e., reduced textile-substrate slip, especially for basalt and steel at 200 °C. According to this research, temperature exposure did not seem to affect the failure mode. Similarly, Estevan et al. [36] investigated the effect of preconditioning at 200 °C and 400 °C on carbon and polymer-impregnated alkali resistant (AR)-glass textiles applied with a hydraulic lime-based mortar on masonry walls. According to their findings, the failure mode switched from textile rupture (provided a sufficient bonded length) to textile slippage at 200 °C (regardless of the bonded length), which was ascribed to the complete degradation of the matrix-textile bond despite the bond capacity was partially retained (maximum loss of 34 %). Ferretti et al. [37] reported on the bond behavior of a basalt FRCM applied onto masonry walls. As in the case of Raoof and Bournas [33], mechanical testing was conducted at the target temperature. A very slow heating ramp was considered, and temperatures up to 80 °C were investigated. The stiffness and the bond capacity weakened drastically as the temperature

increased, and the failure mode shifted from fiber rupture to textile slippage. An overview of test protocols and set-ups hitherto available in the literature on FRCM-masonry joints exposed to thermal conditioning is outlined in Table 1. Among studies presented in Table 1, only in one case the effect of textile impregnation along with exposition to elevated temperature was investigated [28]. However, the bonded length considered might not be sufficient to fully develop the composite stress-transfer mechanism, based on the available literature on this topic [38].

In this paper, the bond behavior of carbon FRCM composites applied to a masonry substrate was investigated after thermal preconditioning. Specimens were subjected to a heating ramp up to 300 °C. Isothermal conditions were then maintained for one hour. The FRCM consisted of a carbon biaxial textile coupled with a commercially available fiber-reinforced cement-based matrix for masonry retrofitting. Spotlight was set on the assessment of the role of a thin diluted epoxy coating applied to the carbon textile on the FRCM-masonry bond capacity, failure mode, and residual load-bearing capacity. To this aim, 16 single-lap direct shear tests were performed. The results show that thermal pre-conditioning has higher detrimental effect on impregnated than on bare textiles. However, the bond capacity obtained with preconditioned impregnated FRCM still outperformed that obtained with bare textile FRCM. This result confirms the shielding role played by the matrix that prevents the organic coating from carbonizing. Furthermore, the thermal preconditioning did not affect the failure mode observed, which remained different between impregnated and bare textile FRCMs.

2. Materials and methods

2.1. Raw materials

The FRCM reinforcement investigated in this work consisted of a carbon textile and a commercially available cement-based mortar matrix. The geometrical and mechanical properties of the biaxial balanced open square-grid carbon fabric are reported in.

Table 2, as declared by the manufacturer [40]. The matrix was a thixotropic cementitious mortar with embedded pre-mixed dispersed AR-glass microfibers specifically designed for masonry substrates [41]. According to the manufacturer datasheet [41], the matrix featured minimum compressive (f_{mc}) and flexural (f_{mf}) strength of 20 MPa and 3.5 MPa, respectively, as well as an apparent density in the fresh state (according to EN 1015–6 [42]) of 1750 kg/m^3.

Both bare (Fig. 1a) and impregnated (Fig. 1b) carbon textiles were

Table 2
Geometrical and mechanical properties of the reinforcing textile and fiber as declared by the manufacturer [40].

Characteristic	Unit	Value
Grid size, i_f	mm	8
Total weight (bare fabric)	g/m^2	200
Weight along warp (weft)	g/m^2	100 (100)
Equivalent thickness, t_f	mm	0.056
Tensile strength of the fiber	MPa	5100
Ultimate elongation of the fiber	[%]	2.1
Elastic Modulus of the fiber	GPa	245
Density of the fiber	g/cm^3	1.78

Table 1
Summary of relevant studies on bond behavior of FRCM applied on brick/masonry elements subjected to thermal conditioning.

	Donnini et al. [28]	Maroudas and Papanicolaou [32]	Ombres et al. [35]	Askouni et al. [21]	Ferretti et al. [37]	Askouni et al. [39]	Estevan et al. [36]
Test set-up	Double-lap shear	Single-lap shear	Single-lap shear	Single-lap shear	Single-lap shear	Single-lap shear	Single-lap shear
Substrate	Single brick	Masonry wall	Masonry wall	Masonry wall	Masonry wall	Masonry wall	Masonry wall
Substrate preparation	n.a.	Moistened	n.a.	Moistened	Moistened	Moistened	Moistened
Fibers	Carbon (with and without polymer coating)	AR-glass	Steel, basalt (2 types), PBO	AR-glass	Basalt	AR-glass	Carbon and AR-glass (polymer-coated)
No. of layers	1	1	1	1, 2	1	2	1
Mortar	Cement-based	Cement-based	Cement-based and NHL with geopolymers	Lightweight e normal weight cement-based mortar	NHL-based	Cement-based and alkali activated	NHL-based
Curing time* [days]	28	28 (7 MC + 21 LC)	≥7	28 (7 MC + 21 LC)	28	28 (7 MC + 21 LC)	60 (7 MC + 53 LC)
Bonded length [mm]	100	50, 75, 100, 125, 150, 175, 200, 225, 250	300	250	300	250	150, 250
Temperatures [°C]	120	100, 200, 300	100, 150, 200	120, 200	32, 40, 50, 60, 80	200, 400	20, 200, 400
Heating rate [°C/min]	n.a.	75	2	75	0.5	7	10
Isothermal phase time [h]	100	1	3	1	3–4	1	1
Cooling rate	No / natural	Slow**	Natural (LC)	Slow**	No	Slow**	Slow**
Test temperature	Ambient / ≥90 % target temperature	Ambient	Ambient	Ambient	Target temperature	Ambient	Ambient
Test speed [mm/min]	0.50	0.30	0.18	0.30	0.15	0.30	0.30
FRCM width [mm]	60	120	55, 50, 50, 60	120	64	120	100
Number of fiber bundles [-]	3	9	17, 3, 6, 6	7	4	7	8, 3
Textile cross-sectional area A_f [mm]	3.12	8.64	9.14, 1.63, 3.30, 2.76	6.55, 13.1	2.18	13.1	3.84, 4.56
Equivalent thickness t_f [mm]	0.052	0.072	0.168, 0.032, 0.064, 0.047	0.055, 0.11	0.034	0.11	0.038, 0.046

*MC = moist curing; LC = laboratory conditions; **=within the switched-off furnace.
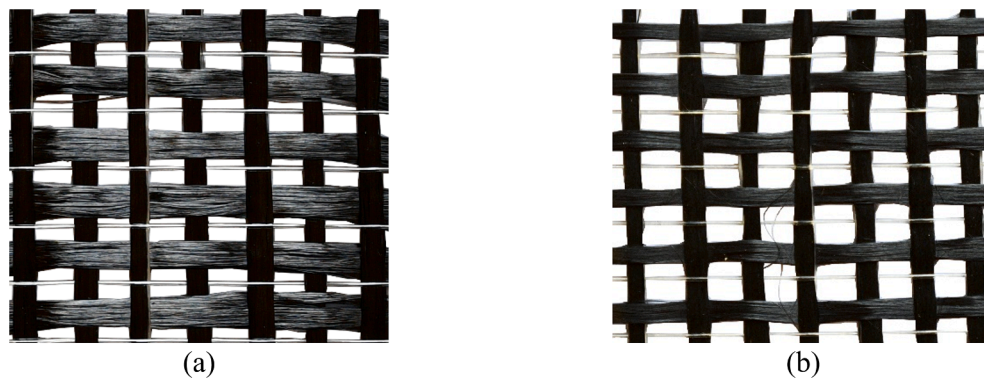
(a)
(b)

Fig. 1. Photo of carbon textile employed: a) bare and b) impregnated textile.

considered in this work. The impregnated carbon textile was manufactured with ultralow viscosity epoxy resin according to the guidelines provided in Signorini et al. [5], under the label EW-75. This coating was realized by diluting at laboratory temperature the epoxy precursor, namely Bisphenol A diglycidyl ether (DGEBA), with acetone at 75 %wt. An aliphatic catalyst (diethylenetriamine) was added to DGEBA in stoichiometric ratio to trigger polymerization of the compound. Previous studies of the hardened resin, including differential scanning calorimetry (DSC) analyses, indicated that its degree of polymerization was 96 % at room temperature (see Messori et al. [29], Fig. 11b, label "EW"). According to the traditional calorimetric approach originally proposed by DiBenedetto [43], the glass transition temperature (T_g) of this resin was computed as 133 °C based on the extent of polymerization. This T_g value is in agreement with the findings of Marks and Snelgrove [44].

Cut-to-size carbon fabrics were rapidly immersed in the epoxy solution, and then squeezed to remove the excess of resin. Finally, impregnated strips were cured at ambient temperature for 7 days. The coating thickness of individual filaments was approximately 1.5 μm and was estimated assuming the mass of the resin deposited on the textile sample as evenly distributed on the fiber surface. This assumption can be justified considering the resin low viscosity [45]. The final mass per unit area of the impregnated textile was, on average, 255 g/m² (±3%).

2.2. Specimen manufacturing and testing

2.2.1. Textile and mortar matrix characterization

The tensile properties of the textile were investigated by means of six uniaxial tensile tests on carbon textile strips with and without the epoxy coating, following the prescriptions of the European EAD 340275–00-0104 [19] and of the Italian AC for FRCM composites [18]. The 420 mm-long and 60 mm-wide specimens comprised $n = 7$ longitudinal bundles. The cross-sectional area of a single fiber bundle was $A^*=0.48$ mm² while the cross-sectional area of the textile was $A_f = nA^*=3.36$ mm². Square-GFRP tabs with side of 60 mm were glued to the specimen ends with epoxy resin to allow gripping by the wedges of the universal testing machine. The free length of the specimens was 300 mm. Tests were conducted in displacement (stroke) control at 0.5 mm/min while recording the applied load, P, and the crosshead displacement, δ. A 100 mm-gauge length extensometer was applied to the central portion of the specimen to measure the axial strain, ε. The axial stress, σ, was computed as the ratio between the load measured by the testing machine, P, and the cross-sectional area of the textile, A_f. In this paper, textile stresses were computed always with respect to the bare fiber cross-sectional area, regardless of the presence or not of the impregnation [17,27].

Following EN 1015–11 [46], the mechanical properties of the mortar matrix were obtained by performing 12 three-point bending tests followed by 24 compression tests. The specimens for bending test had a 40 × 40 mm cross-section and a length of 160 mm. The test span was 100

mm. Compressive tests were performed on the (24) failed half-prisms through a 40 mm-sided square die.

2.2.2. Direct shear tests

Following the Italian AC for FRCM composites [18], 16 carbon FRCM-masonry joints were tested using a single-lap direct shear test setup (Fig. 2). To this aim, fired clay brick masonry walls were manufactured. The walls had 120 × 110 mm nominal cross-section, and nominal height of 380 mm. Each wall was made stacking six half UNI bricks [47] with nominal dimensions (prior to cutting in half) 240 × 110 × 60 mm with 10 mm-thick lime-based mortar joints. As declared by the manufacturer, the brick mean compressive strength when the load is orthogonal to the 240 × 110 mm face, $f_{b,cv}$, was equal to 18 MPa, while the mean compressive strength measured orthogonal to the 240 × 40 face, $f_{b,ct}$, was 2.2 MPa [47]. The lime-based mortar joints compressive strength was $f_{cm} = 2.5$ MPa [48].

FRCM-masonry joints were manufactured by applying the FRCM strip onto the 120 mm-wide surface of the masonry wall, which had been previously completely soaked in water for at least 30 min. FRCM strips were applied at 30 mm from the edge of the masonry wallet. The geometry of the specimen is reported in Fig. 2a. Polytetrafluoroethylene (Teflon) formworks were employed to control the strip size (see Fig. 3a). First, a 4 mm-thick (internal) mortar layer was applied to the wall surface and properly levelled with a trowel. Then, cut-to-size carbon textile strips comprising $n = 7$ axial fiber bundles were gently pressed onto the fresh mortar to promote proper impregnation. A second 4 mm-thick (external) layer of mortar was immediately cast over the textile (see Fig. 3b). The total thickness of the FRCM strip was $t = 10$ mm, the width $b_f = 60$ mm, and the FRCM-masonry joint bonded length was $L = 300$ mm. The width of the FRCM strip was selected to comprise the same number of bundles of the specimens employed for the textile tensile tests (see Section 2.2.1), as prescribed by the Italian AC for FRCM composites [18]. The specimens were left to cure at laboratory conditions (temperature and relative humidity of approximately 23 °C and 60 %, respectively) for at least 28 days. A portion of textile was not embedded in the cementitious matrix at the free (30 mm) and at the loaded (270 mm) ends. GFRP tabs were epoxy glued to the bare textile end to be clamped by the testing machine. Prior to preconditioning, an insulating rock-wool layer was applied to protect the bare textile emerging from the matrix at the loaded and free ends of the FRCM-masonry joints (see Fig. 3c).

During test, the masonry block was restrained to the testing machine with a steel frame specifically designed to prevent displacements and rotations of the specimen, whereas the textile was pulled (Fig. 2). Details regarding the features of the pull–push single-lap shear test can be found in [49]. The test was conducted in displacement (stroke) control at a rate of 0.2 mm/min. Two pairs of linear variable differential transformers (LVDTs) were attached to the masonry wall on the side of the FRCM strip at the loaded and free ends and reacted-off of L-shaped aluminum plates
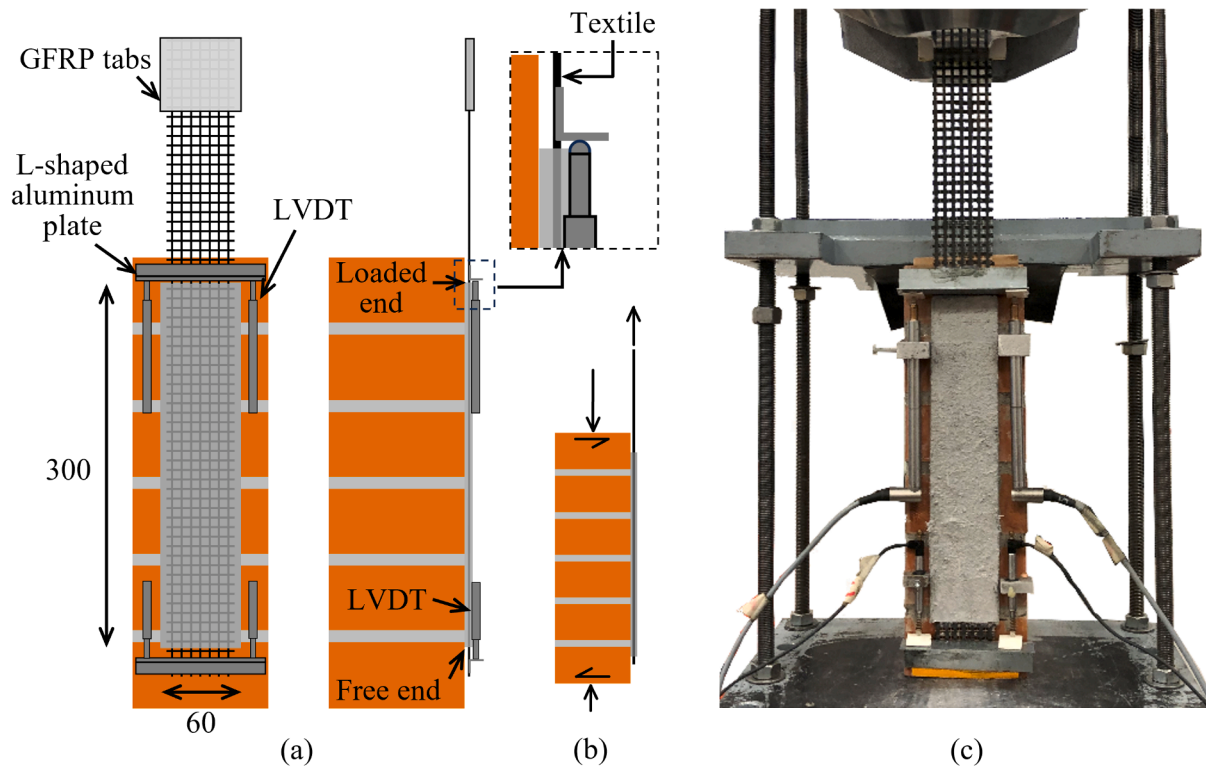
Fig. 2. Direct shear test set-up: a) sketch of the specimen geometry (dimensions in mm), b) free body diagram, and c) photo of a control specimen with bare textile.
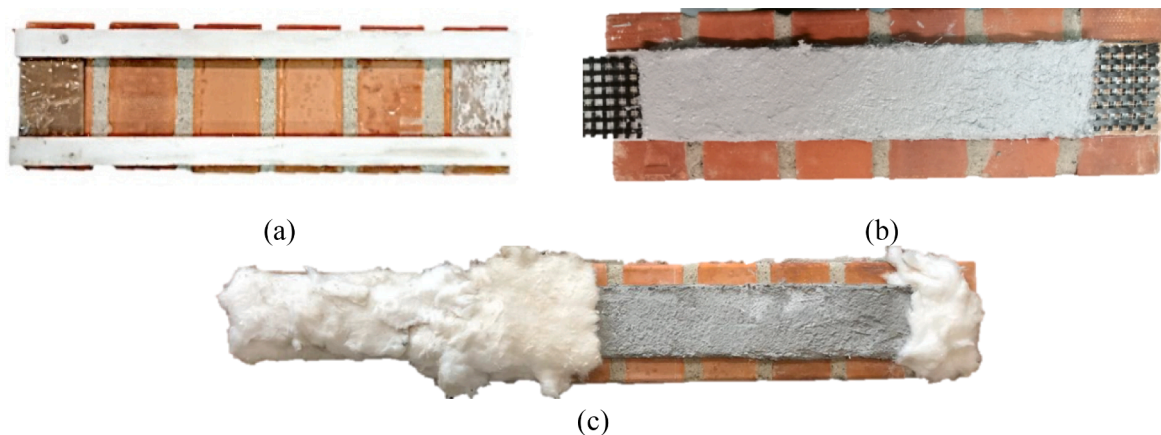

Fig. 3. Manufacturing steps: (a) Teflon formwork; specimen (b) after curing at laboratory conditions, and (c) before the thermal preconditioning.

attached to the textile right outside the FRCM strip (see Fig. 2). The first pair, with 20 mm-stroke range, recorded the relative displacement between the textile and substrate at the loaded end and their average value is referred to as the global slip, g, in this paper. The remaining pair of LVDTs, having a 10 mm-stroke range, recorded the relative displacement between the textile and substrate at the free end. Their average defines the free end slip, g_f. The fiber axial stress, σ, was computed as the ratio between the load applied by the testing machine P and the fiber cross-sectional area $A_f = t_f\, b_f$. It is worth noting that, being $t_f = nA^*/b_f$, the fiber cross-sectional area A_f is the same as that computed in Section 2.2.1 (i.e., $t_f b_f = nA^*$).

2.3. Thermal preconditioning protocol

Six bare textile strips, six mortar prisms (Fig. 4a), and eight FRCM-masonry joints (Fig. 4b) were subjected to thermal preconditioning as

hereinafter detailed. After 28-day curing, the mortar prisms and the FRCM-masonry joints were inserted in an electrical oven for 250 min overall, where they laid horizontally to be heated up to 300 °C [32]. The thermal preconditioning protocol consisted of an initial heating ramp up to 200 °C with a rate of 3 °C/min followed by 80 min at the constant temperature of 200 °C. A second heating ramp with a rate of 2 °C/min was subsequently applied up to 300 °C. The final conditioning temperature (300 °C) was maintained for 60 min. Specimens were allowed to cool naturally for 24 h in the switched-off oven, until laboratory temperature (approximately 24 °C) was reached. This protocol was selected to study the influence of the elevated temperature as well as of the exposure time [50], the latter being used as an indicator to assess integrity and stability of buildings in fire safety design [24]. The furnace air temperature was continuously monitored using the oven built-in sensor, as well as with two K-type thermocouples that were placed close to the surface of the specimens. This redundancy was introduced to
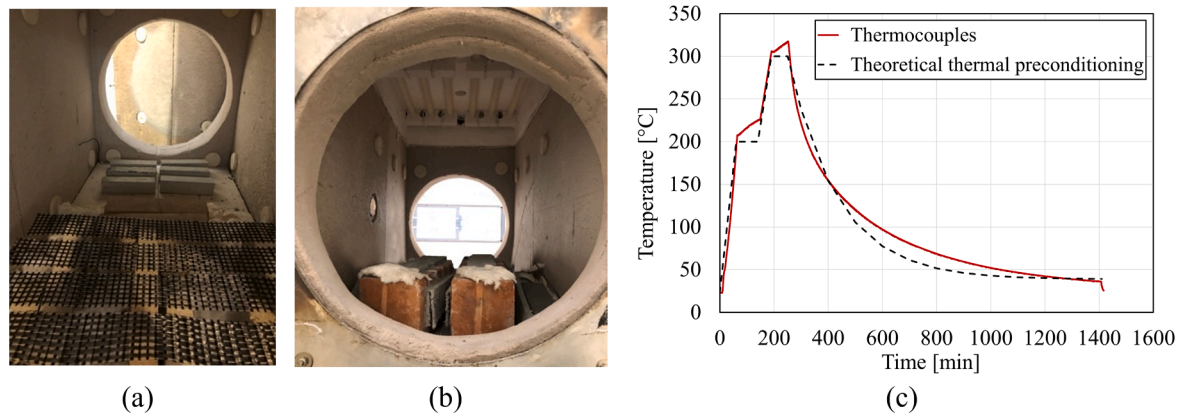
Fig. 4. Experimental set-up for thermal ageing of (a) textile and mortar matrix specimens and (b) FRCM-masonry specimens. (c) Thermal preconditioning protocol.

accurately measure the temperature at which the specimens were exposed. Fig. 4c presents both the prescribed (as measured by the built-in sensor of the furnace) and the recorded time–temperature profiles, the latter being the average of the thermocouples output.

Although some differences can be observed between the two curves due to the thermal inertia of the furnace, they can be considered small in comparison with the conditioning temperature. In fact, the maximum temperature recorded by the thermocouples reached 320 °C, which is only 6 % higher than the target temperature of 300 °C.

3. Results and discussion

3.1. Textile tensile tests

Fig. 5 presents the stress σ – strain ε curve for the 12 textile specimens tested in tension. Specimens were labelled T-C-X-Y-C-T-N, where T = tensile test, C = carbon fabric, X = specimen free length (in mm), Y = specimen width (in mm), C (if present) = presence of coating, T (if present) = the specimen was exposed to the thermal conditioning procedure, and N = specimen number.

The results of the tensile tests of control bare textile specimens are gathered in Table 3, where the tensile strength, $\sigma_{f,u}$, ultimate strain, $\varepsilon_{f,u}$, and fiber elastic modulus, E_f, are presented for each specimen. E_f was determined as the secant modulus of the σ – ε curve between $\sigma_{f,1} = \sigma_{f,u}/10$ and $\sigma_{f,2} = \sigma_{f,u}/2$ [18]. Average values and coefficients of variation (CoV) for each group of nominally equal specimens are also reported in Table 3. The results of bare and impregnated textiles subjected to the thermal preconditioning described in Section 2.3 are provided in Table 4.

Table 3
Tensile test results of control bare and impregnated carbon textiles.

Specimen	$\sigma_{f,u}$ [MPa]	$\varepsilon_{f,u}$ [%]	E_f [GPa]	Specimen	$\sigma_{f,u}$ [MPa]	$\varepsilon_{f,u}$ [%]	E_f [GPa]
T-C-300-60-1	1933	0.97	205	T-C-300-60-C-1	2811	1.51	231
T-C-300-60-2	1884	1.08	204	T-C-300-60-C-2	3111	1.87	213
T-C-300-60-3	1876	0.98	207	T-C-300-60-C-3	3125	1.66	219
Average	1897	1.01	206	Average	3016	1.68	221
CoV [%]	1.32	4.74	0.52	CoV [%]	4.81	8.87	3.37

Table 4
Tensile test results of preconditioned bare and impregnated carbon textiles.

Specimen	$\sigma_{f,u}$ [MPa]	$\varepsilon_{f,u}$ [%]	E_f [GPa]	Specimen	$\sigma_{f,u}$ [MPa]	$\varepsilon_{f,u}$ [%]	E_f [GPa]
T-C-300-60-T-1	1595	0.80	205	T-C-300-60-C-T-1	2185	1.06	198
T-C-300-60-T-2	1642	0.90	205	T-C-300-60-C-T-2	2154	1.24	175
T-C-300-60-T-3	1358	0.97	157	T-C-300-60-C-T-3	2515	1.11	211
Average	1532	0.89	189	Average	2285	1.14	195
CoV [%]	8.11	7.70	11.94	CoV [%]	7.15	6.54	7.57

A significant contribution of the epoxy impregnation can be observed both in the control and in the preconditioned group. In particular, the presence of coating led to higher tensile strength and ultimate strain values. The average tensile strength for bare and impregnated specimens in the control group was $\bar{\sigma}^* = 1897$ MPa and $\bar{\sigma}^* = 3016$ MPa, respectively (increase of 58.9 %). This considerable increase in the tensile strength of the impregnated textiles was attributed to the binding action of the epoxy resin, which promoted an even stress redistribution among
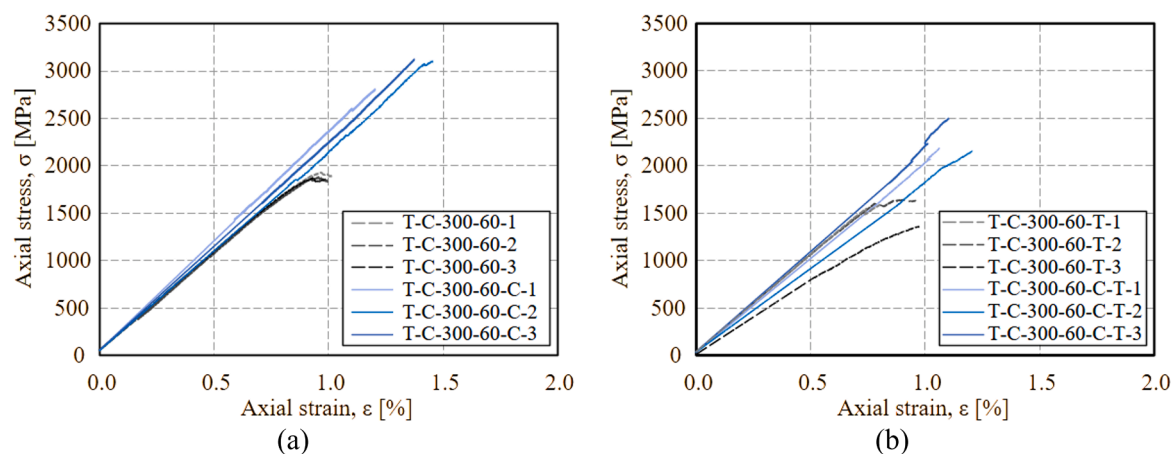

Fig. 5. Axial stress–strain curves obtained for (a) control and (b) preconditioned carbon textiles.

fiber filaments within the bundle [51]. Although to a lesser extent, a similar enhancement could also be observed in the preconditioned group, for which the tensile strength varied from $\overline{\sigma}^* = 1532$ MPa to $\overline{\sigma}^* = 2285$ MPa for impregnated and dry specimens, respectively, with a 49.1 % increase. The coating did not significantly affect the textile elastic modulus, which showed variations in average values of 7.4 % for the control and 3.0 % for the preconditioned group. The improvement of the textile tensile behavior due to the presence of impregnation was previously reported in the literature for FRCM comprising different textiles (e. g., [52]).

For bare specimens, it was observed that the average tensile strength after conditioning remained equal to 80.8 % of that in the control group. The corresponding comparison for impregnated specimens showed that conditioning led to an average tensile strength equal to 75.8 % of that in the control group. Hence, thermal preconditioning affected the tensile strength of the textile in a similar manner for bare and impregnated textiles. A decrease of ultimate strain was observed for bare (-11.9 % for average values) and impregnated (–32.1 % for average values) textiles after the preconditioning. A modest reduction of E_f was observed, namely −8.0 % for bare and −11.7 % for impregnated textiles. These results confirm that impregnated textiles are generally more vulnerable to thermal preconditioning than dry textiles. Although this detrimental effect may be connected to the epoxy well-known sensitivity to high temperature, it appeared less pronounced than expected.

Fig. 6 shows an optical investigation of the textile after thermal conditioning (Fig. 6b and c) compared to the control group (Fig. 6a). For both bare and impregnated textiles, the polymeric thermoplastic stitches used for textile thermo-welding underwent a carbonization process and appeared black and partially molten as a result of thermal conditioning. In contrast, the bare textile appeared to suffer little damage by elevated temperature exposure. The typical failure mode for the dry textile consisted in subsequent failures of fiber filaments of different longitudinal bundles (Fig. 7a), as opposed to the abrupt tensile failure of the longitudinal bundles for the impregnated textile, usually anticipated by the rupture of some knitting points connecting transverse and longitudinal bundles (see Fig. 7b).

3.2. Mortar matrix bending and compression tests

Bending tests were performed on six control specimens and provided a mortar average flexural strength of 7.1 MPa (CoV = 16.5 %). Compression of the 12 half specimens obtained after failure in bending provided a mean compressive strength of 37.5 MPa (CoV = 4.2 %).

A visual comparison between the fractured cross-sections resulting from the bending test of control and preconditioned specimens is illustrated in Fig. 8. First, a distinct change in color was observed, which is
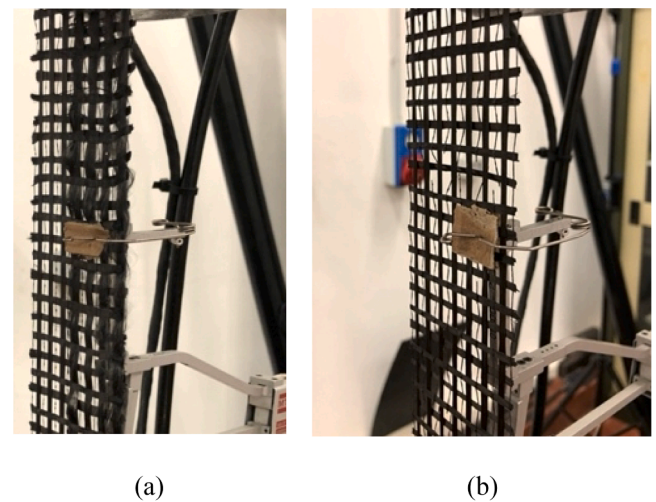
(a)　　　　　　(b)

Fig. 7. Failure modes for preconditioned (a) bare and (b) impregnated textiles.

due to the de-hydration of the binder and modification of the aggregates [53]. In particular, silicate aggregates tended to acquire a reddish nuance [54]. The average flexural strength obtained by preconditioned specimens was 4.2 MPa (CoV = 10.4 %, computed on six specimens), while the average compressive strength was 31.1 MPa (CoV = 4.9 %, 12 specimens), which entails for a 40.3 % reduction of flexural strength and a 17.1 % reduction of compressive strength. The decrease of mechanical properties of cementitious mortars was expected, as conditioning at elevated and high temperature leads to a loss of free and absorbed water, which is responsible for higher and generally wider porosity, promotion of micro-sized crack formation, and differential volumetric changes between paste and aggregates (see Fig. 8). Besides, thermal decomposition of the paste and desiccation of C-S-H gel, already taking place at moderate temperatures (beyond approximately 105 °C [55]), impairs the strength capacity of the cementitious paste [56,57]. Still, as expected, results highlighted that the detrimental effect on the compressive strength of the cementitious mortar remained limited, whereas the impact on the flexural strength was more significant. This result was mainly ascribed to the peculiarity of bending behavior, which mostly relies on the performance of a small fraction of the material, and it is therefore more prone to deviation. Besides, the deterioration of the bond between the dispersed short glass fibers and the surrounding matrix could have affected the results. Indeed, Colombo et al. [58] pointed out a significant decay of the bending strength of fiber-reinforced cement-based composites after exposure to temperatures between 200 °C and
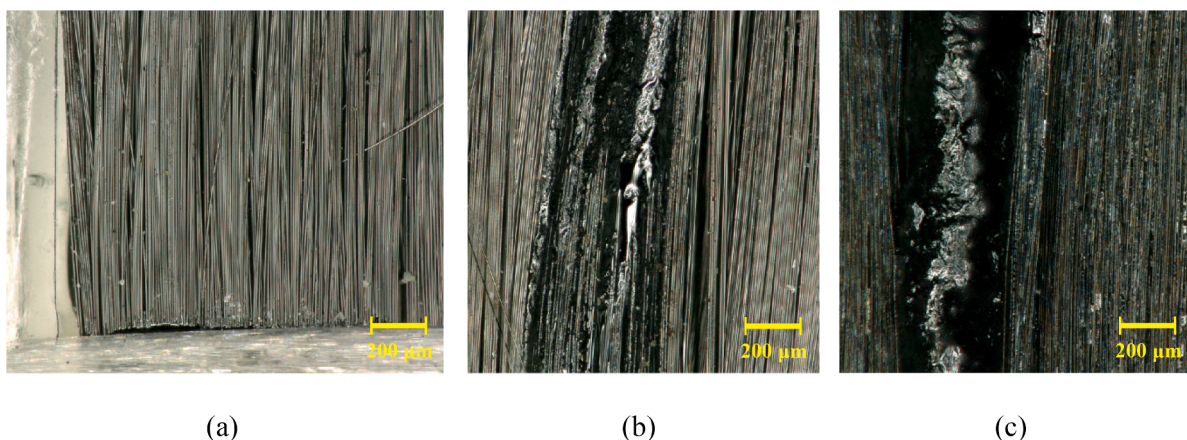
(a)　　　　　　(b)　　　　　　(c)

Fig. 6. Optical microscopy investigation of textiles: (a) control and (b) preconditioned bare textile; (c) preconditioned impregnated textile (Note: the thick wire is the thermo-welding polymeric stitching element).
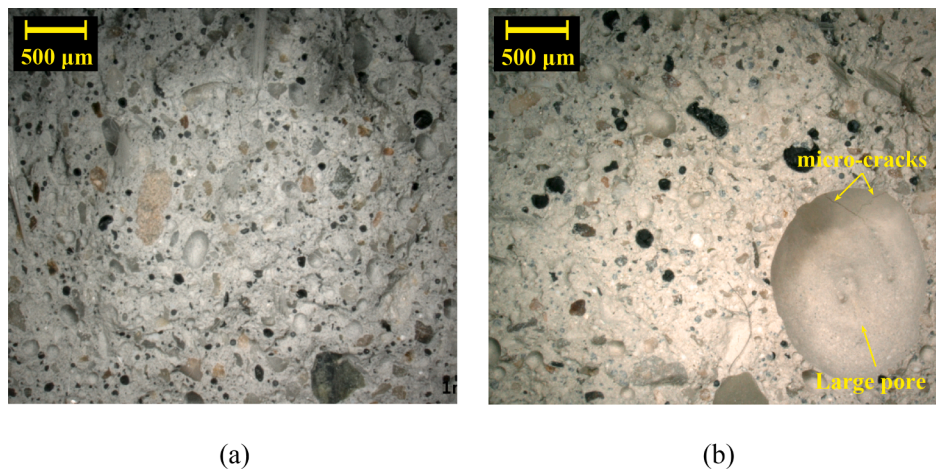
Fig. 8. Optical microscopy investigation of the cross-section of (a) control and (b) preconditioned mortar matrix specimens after testing.

400 °C, while the compressive strength was only marginally affected. These findings were attributed to the deterioration of the bridging capacity of the dispersed fibers, which were reported to play a key role in determining the mortar tensile and bending capacity. A visual comparison of the interphase zone between AR-glass fibers and the surrounding matrix is shown in Fig. 9.

Although a conclusive statement on the fiber bridging capacity can hardly be made – and lies beyond the scope of this study – it could be observed that cracks surrounding the fibers were visible for preconditioned samples, and they generally appeared wider than those in the control group. This fact seems to support the idea that some damage at the fiber-mortar interface may occur during the preconditioning.

3.3. Direct shear tests

3.3.1. Control specimens

Fig. 10a shows the axial stress σ – global slip *g* curves obtained from single-lap direct shear test of control bare and impregnated textile FRCM-masonry joints. Fig. 10a shows that the effect deployed by the impregnation was consistently remarkable, both in terms of peak stress enhancement as well as in failure mode shifting. Indeed, the improved matrix-textile interface properties combined with the monolithic response of the carbon longitudinal bundles resulted in peak stresses that were nearly twice those of the control specimens (89.3 % increase in average value). This improvement reflected a difference in the failure mode. Specimens with bare textile showed progressive slippage of the textile with respect to the matrix (debonding at the matrix-textile

interface) and failure of some outermost filaments (i.e., the sleeve filaments). Specimens with impregnated textile failed due to the sudden opening of a matrix crack (either longitudinal at the matrix-textile interface or transversal from the external toward the internal matrix layer - or both) that triggered matrix interlaminar failure. In this case, the internal matrix layer remained bonded to the masonry wall.

The average peak stress of control specimens, computed with respect to the bare fiber cross-sectional area, was $\overline{\sigma}^* = 968$ MPa, well below the average tensile strength of the bare carbon fabric $\overline{\sigma}_{f,u} = 1897$ MPa (see Table 3), thus providing an exploitation ratio of 51.0 %. Indeed, as it usually happens for bare textile FRCMs, large slippage was observed at the matrix-textile interface. Then, progressive filament failure occurred, starting from the sleeve ones. As well known, impregnation of the bundle filaments by the hydration products of the binder is limited, which leads to premature stiffness reduction and to the residual behavior being mainly governed by friction [59]. Fig. 11 shows the typical failure mode of bare textile FRCM-masonry joints, clearly revealing that transversal bundles remained embedded in the matrix while longitudinal bundles were progressively pulled out from it. The slippage mechanism of the longitudinal bundles was also detected by the LVDTs at the free end, i.e., by the slip at the free end g_f.

The σ – *g* curves of bare carbon FRCM-masonry joints closely resembled the trend already described by D'Antino et al. [60] and analytically modeled in the literature (see e.g., [59,61]). Accordingly, the initial ascending branch, which describes the elastic response of the fully bonded system, was followed by a non-linear branch with decreasing slope associated with irreversible phenomena taking place in
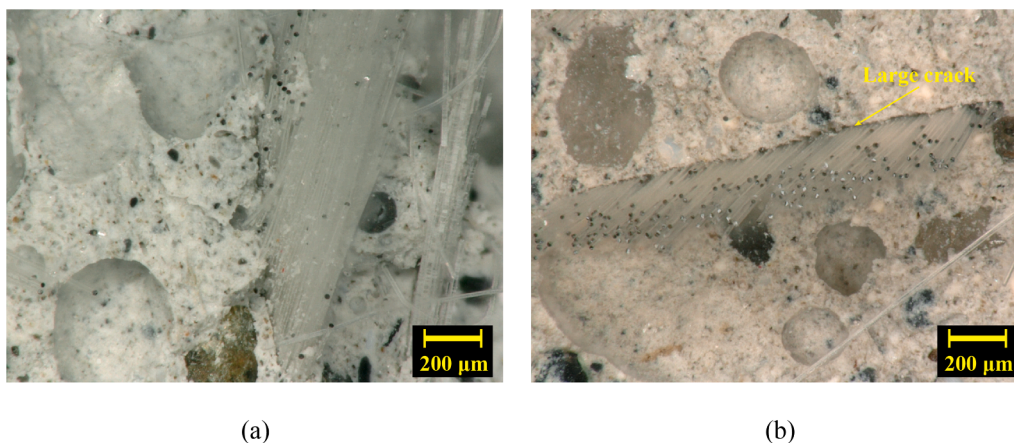

Fig. 9. Optical magnification of the interaction area (interphase zone) between dispersed AR-glass fibers in (a) control and (b) preconditioned mortar.
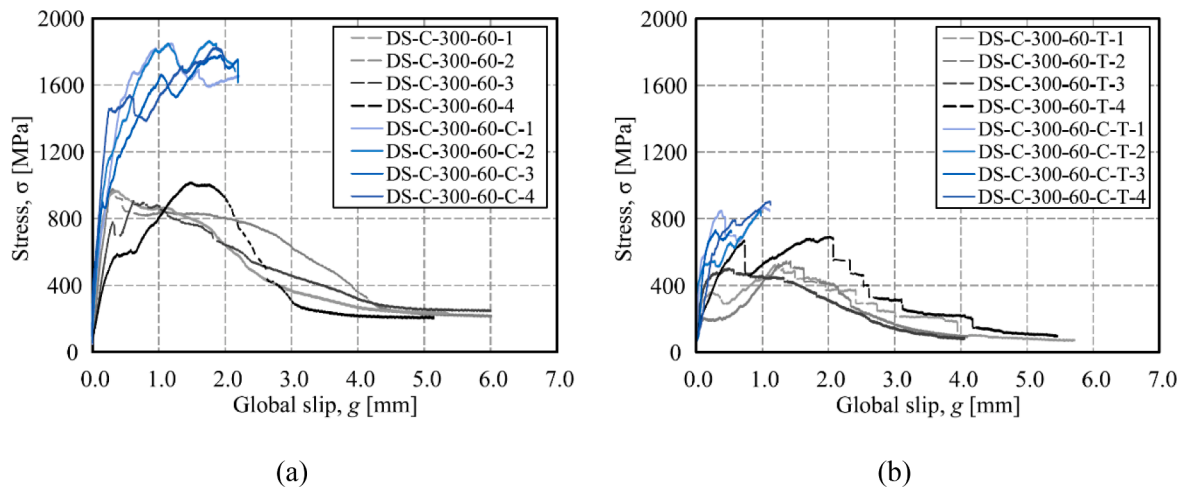
Fig. 10. Stress versus global slip curves for (a) control and (b) preconditioned FRCM-masonry joints.

Fig. 11. Failure mode for a (control) bare textile FRCM-masonry joint (DS-C-300-60-1). Slippage of longitudinal bundles was observed without the formation of matrix crack.

the joint. At the end of this branch, the bond stress-transfer mechanism was assumed as fully established and debonding occurred at the loaded end. The stress attained at this point was defined as the debonding stress (σ_{deb}). As debonding propagated along the joint, further increase in the applied stress was observed, owing to the contribution of friction at the matrix-textile interface, until the attainment of the peak stress σ^* [60,62]. The decreasing branch of the curve was followed by a plateau indicating that the applied stress was balanced by friction only, i.e., full matrix-textile debonding occurred [63]. The presence of friction in the final branch of the σ-g curve was reported in various studies for various bare textile FRCMs [64–66].

In contrast, impregnated specimens consistently failed due to sudden cracking of the matrix after debonding at the matrix-textile interface (matrix interlaminar failure). As a result, the experimental curves in Fig. 10a diverge from the idealized response after the attainment of the debonding stress σ_{deb} (a similar result was observed for impregnated

textiles in Raoof et al. [67]). Indeed, the peak stress σ^* was reached for higher values of the global slip compared with those of corresponding bare textile FRCM. This may be explained by the absence of telescopic failure in the impregnated bundles, which behaved monolithically. Once this limiting stress σ^* was reached, the textile suddenly detached from the matrix and failure occurred, resulting in a considerable amount of elastic energy being stored in the system and then subsequently released in a concentrated burst upon failure.

Fig. 12 shows the typical failure mode exhibited by FRCM-masonry joints with impregnated textile. Half of the tested specimens exhibited longitudinal mortar cracks at the matrix-textile interface at the loaded end. This behavior is similar to what is generally observed for steel-reinforced grout (SRG), where matrix interlaminar failure is often observed [68].

It is worth noting that also for specimens with impregnated textile, the tensile strength of the material could not be completely exploited in direct shear tests. Indeed, the average value of the σ – g curves peak stress for impregnated specimens was $\overline{\sigma}^* = 1831$ MPa. Comparing this result with the average tensile strength measured for the same impregnated carbon textile (see Table 4), an exploitation ratio of 60.7 % was obtained. However, comparing results for impregnated and bare textile specimens, it was found that the coating allowed for increasing the exploitation ratio due to enhanced bond within the bundle and between bundles and matrix. Similar observations were reported in the literature for different FRCMs [69].

Table 5 and Table 6 gather the values of peak load and stress attained by each specimen in the bare and impregnated group, respectively, as well as the corresponding value of global slip, g^*, and the failure mode.
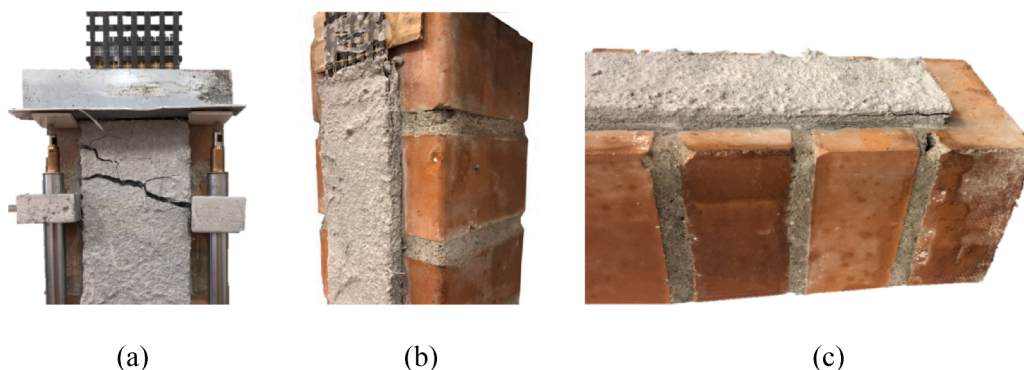

Fig. 12. Failure modes of (control) impregnated FRCM specimens: loaded end of specimen (a) DS-C-300-60-C-1 and (b) DS-C-300-60-C-2; (c) matrix interlaminar crack at the free end of specimen DS-C-300-60-C-1.

Table 5 also provides the residual friction stress σ_f, defined as the average of stress values of the $\sigma - g$ curve for which $200 \leq d\sigma/dg \leq 0$ holds [61,70]. The residual friction stress was reported only for specimens that exhibited fiber slippage until completion of the test. Comparing results obtained for specimens with impregnated and bare textiles, an 89.3 % enhancement in average bond capacity was observed for the former over the latter. Similar results were obtained for the corresponding global slip, which in impregnated textile FRCM-masonry joints exhibited a 144 % increase with respect to the bare textile FRCM-masonry joint counterparts. Interestingly, although data scattering was narrow in both specimen groups, the presence of coating was associated with a lower variance. This indicates that coating promoted a more consistent failure mechanism, which can be attributed to the more even and more consistent distribution of the external load within and among impregnated bundles.

3.3.2. Effect of thermal preconditioning on bond properties

Fig. 13 shows failed preconditioned bare textile FRCM-masonry joints after testing. In these tests, pronounced fiber slippage of longitudinal bundles occurred along with telescopic failure [63]. Furthermore, transversal bundles generally remained embedded in the matrix and were partially pulled off of the composite in the vicinity of the loaded end only for some specimens (Fig. 13b). Slip measurements at the free end confirmed that pronounced slippage took place. In some specimens, matrix interlaminar failure was also observed (Fig. 13b). The thermal preconditioning was associated with a reduction of peak stress (reduction of average value of 58.6 %) and an increase in data scattering with respect to control specimens.

The slope of the specimen response in the post-elastic regime, up to peak stress, appeared reduced to some extent (see Fig. 10b). As expected for bare textiles, fibers appeared undamaged by temperature conditioning. Remarkably, absence of damage was observed for epoxy-impregnated textiles as well, as documented in Fig. 14, which shows the failure mode of specimen DS-C-300–60-C-T-1. The detrimental effect of the preconditioning seemed mainly restricted to the matrix-textile interface and to the mortar. Indeed, while fibers did not appear affected by preconditioning, at least by visual inspection (see Fig. 14c), the interface between the mortar layers, accommodating the textile, consistently turned to a darker color with respect to the external matrix surface (see Fig. 14d).

This was also confirmed by the results reported in Section 3.1 and 3.2, according to which the mechanical properties decreased for preconditioned mortar specimens (particularly in terms of flexural strength). The thermal preconditioning was responsible for a significant reduction of the bond capacity in FRCM-masonry joints with impregnated textile (-54.1 % on average values) with respect to the control group (retained strength of 45.9 %). For all impregnated textile specimens, debonding at the interface between the matrix and the textile was observed, alongside several variedly spaced transversal cracks on the external mortar layer (see Fig. 14b). Interestingly, no slippage was detected at the free end, which indicated that debonding did not reach the free end. The overall data scattering, as measured in terms of CoV, remained well below the 10 % threshold, most likely due to the

Table 5

Results of direct shear tests of (control) bare textile FRCM-masonry joints.

Specimen	P^* [kN]	σ^* [MPa]	g^* [mm]	σ_f [MPa]	Failure mode
DS-C-300-60-1	3.29	978	0.30	226	Debonding at the
DS-C-300-60-2	3.25	967	0.36	231	matrix-textile interface
DS-C-300-60-3	3.04	906	0.62	253	associated with fiber
DS-C-300-60-4	3.42	1019	1.48	209	slippage and rupture of
					sleeve filaments
Average	3.25	968	0.69	230	
CoV [%]	4.81		78.64	7.79	

P^*=peak load; σ^*=peak stress; g^*=global slip; σ_f = residual friction stress.

Table 6

Results of direct shear tests of (control) impregnated textile FRCM-masonry joints.

Specimen	P^* [kN]	σ^* [MPa]	g^* [mm]	σ_f [MPa]	Failure mode
DS-C-300-60-C-1	6.22	1851	1.19	–	Debonding at the
DS-C-300-60-C-2	6.27	1866	1.76	–	matrix-textile interface
DS-C-300-60-C-3	5.99	1781	1.93	–	associated with matrix
DS-C-300-60-C-4	6.14	1827	1.86	–	transversal and/or
					interlaminar cracking
Average	6.15	1831	1.69	–	
CoV [%]	2.02		20.10		

P^*=peak load; σ^*=peak stress; g^*=global slip; σ_f = residual friction stress.

(a)   (b)
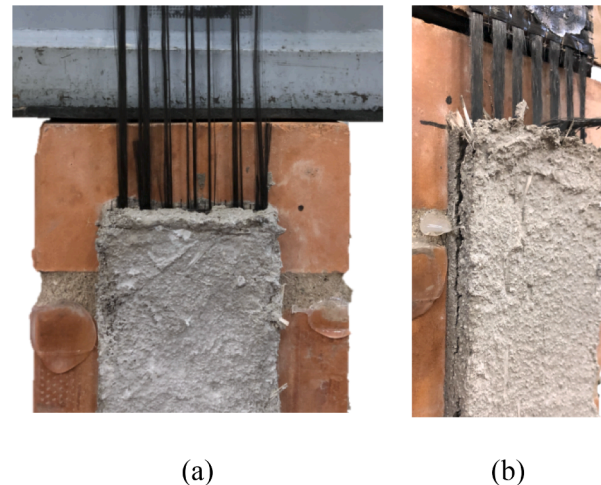
Fig. 13. Failure mode for bare textile FRCM exposed to the temperature preconditioning: (a) fiber slippage and telescopic failure and (b) matrix interlaminar failure.

consistent nature of the failure mode.

In Table 7 and Table 8, the peak load, peak stress, and residual friction stress are reported for the preconditioned specimens, as well as the global slip g^* corresponding to σ^*. The average bond capacity of preconditioned impregnated textile specimens remained 48.2 % higher than that of the bare textile counterparts, which confirmed the important role played by the coating that still held after thermal preconditioning, albeit with lesser efficacy. A higher average value of the global slip associated with the peak stress, $\bar{g}^*$, was obtained for bare rather than for impregnated specimens in the preconditioned group. The thermal conditioning affected the slip behavior in an opposite way for bare and impregnated textiles, leading to an 86.0 % increase of $\bar{g}^*$ for the former, and a 49.6 % decrease for the latter.

Comparing Table 5 and Table 7 (bare textile specimens), a general decrease of σ^* and σ_f can be noted. Namely, the average value of the peak stress and residual friction stress decreased of 41.4 % and 58.7 %, respectively, after preconditioning. An analogous detrimental effect could be observed comparing Table 6 and Table 8 (impregnated specimens), which showed a 54.1 % decrease of $\bar{\sigma}^*$ after preconditioning.

3.4. Degradation mechanism: Microscopy investigation

Fig. 15 and Fig. 16 show a scanning electron microscope (SEM) investigation of the carbon fabric without (bare) and with impregnation, respectively, obtained from the FRCM strengthening layer after temperature preconditioning and mechanical testing.

At this magnification levels, bare fibers presented various orientations, which supported the idea that, in the bare textile, telescopic unfolding of the bundles occurred as fiber debonded and slipped during
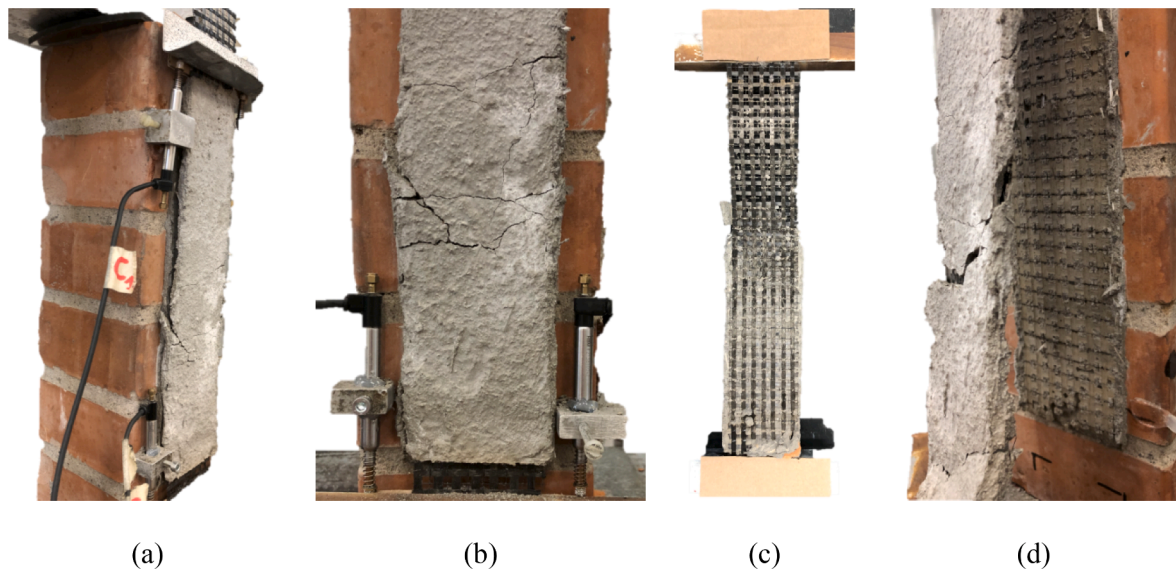
Fig. 14. Failure mode for impregnated textile FRCM specimen DS-C-300-60-C-T-1 exposed to the temperature preconditioning: (a) longitudinal crack at the interface, (b) transversal matrix crack, (c) textile and (d) mortar at the matrix-textile interface.

Table 7
Results of direct shear tests of preconditioned bare textile FRCM-masonry joints.

Specimen	P^* [kN]	σ^* [MPa]	g^* [mm]	σ_f [MPa]	Failure mode
DS-C-300-60-T-1	1.77	526	1.20	82	Debonding at the matrix-textile interface associated with fiber slippage and debonding at the matrix-textile interface associated with matrix interlaminar cracking
DS-C-300-60-T-2	1.83	546	1.42	107	
DS-C-300-60-T-3	1.69	502	0.50	88	
DS-C-300-60-T-4	2.33	693	2.02	102	
Average	1.90	567	1.28	95	
CoV [%]	15.22		48.97	12.26	

P^*=peak load; σ^*=peak stress; g^*=global slip; σ_f = residual friction stress.

Table 8
Results of direct shear tests of preconditioned impregnated textile FRCM-masonry joints.

Specimen	P^* [kN]	σ^* [MPa]	g^* [mm]	σ_f [MPa]	Failure mode
DS-C-300-60-C-T-1	2.92	871	1.04	–	Debonding at the matrix-textile interface associated with matrix transversal and/or interlaminar cracking
DS-C-300-60-C-T-2	2.86	852	0.97	–	
DS-C-300-60-C-T-3	2.46	733	0.30	–	
DS-C-300-60-C-T-4	3.04	904	1.11	–	
Average	2.82	840	0.85	–	
CoV [%]	8.89		44.03	–	

P^*=peak load; σ^*=peak stress; g^*=global slip; σ_f = residual friction stress.

the test. Broken fibers could be observed only occasionally, and the same holds for small mortar patches adhering to fibers. On the contrary, impregnated fibers were clearly aligned in a main direction (i.e., the load direction) both before and after the thermal preconditioning, which indicated that the coating was able to keep the fibers aligned even after the preconditioning. Besides, Fig. 16b provides clear evidence of fiber tensile rupture, which occurrence may have been promoted by the embrittlement of the carbon fibers caused by elevated or high temperature exposure, as mentioned by Sauder et al. [71]. The coating layer

can be clearly seen in Fig. 17 as a thin opaque glaze resting on the filaments and gluing the filaments together and to the matrix. Adhesion of the mortar matrix to the impregnated textile was demonstrated by many scattered binder patches attached to the fiber surface and connecting the bundles together. Despite the performance loss caused by thermal preconditioning, no visual damage could be detected on the fibers by FEG-SEM investigation. The thermal degradation of the epoxy coating due to temperature exposure could be considered as the key factor leading to this performance loss, also because it promoted a transition from brittle to rubber-like behavior for the resin [72]. However, the shielding effect provided by the cement-based matrix was remarkable and prevented oxidation and combustion of the coating, as it was instead reported by de Castro et al. [73].

Elevated temperature exposure also led to degradation of the embedding matrix, in the shape of increased macro porosity, which in turn favored crack initiation and propagation. This is documented by the micrographs in Fig. 18, which compare control and preconditioned matrix collected directly from the FRCM strengthening layers after direct shear testing. Fig. 18 shows an increase in the matrix open porosity after preconditioning.

4. Conclusions

This study investigated the role of diluted epoxy impregnation of carbon textiles on the mechanical performance of FRCM strips for masonry strengthening, with emphasis on assessing the effect of thermal preconditioning of the specimens up to 300 °C for 250 min. The tensile strength of the bare textile as well as the flexural and compressive strength of the mortar matrix were determined both prior and after thermal preconditioning. Direct shear tests were performed to investigate the bond behavior of FRCM-masonry joints depending on the presence of textile epoxy coating and thermal preconditioning. A microscopy analysis was performed to better determine the role of the cementitious matrix in protecting the organic coating from elevated temperature degradation. The results showed that, even though thermal preconditioning proved detrimental to the mechanical performance of bare and, even more, of impregnated textile specimens, the advantages that the latter showed over the former in terms of higher tensile strength and bond capacity were for the most part preserved up to 300 °C. These gains produced a consistent shift in the failure mechanism, from matrix-textile debonding associated with fiber slippage to matrix-textile debonding associated with matrix interlaminar failure. The data

(a)

(b)
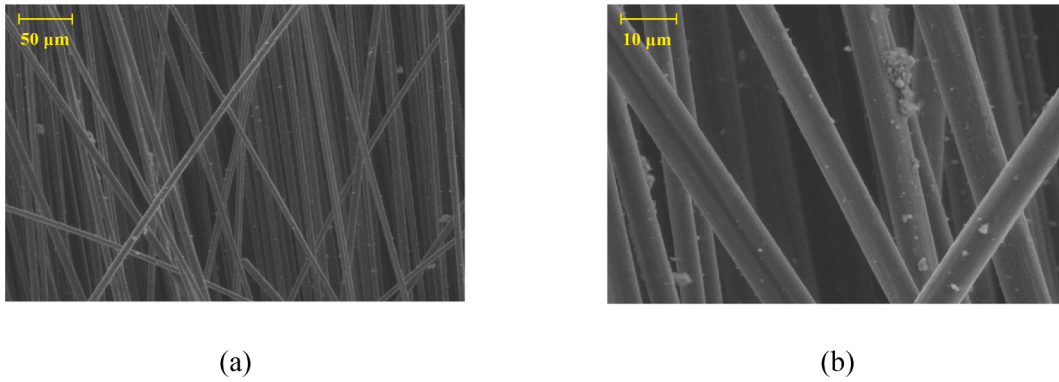
Fig. 15. SEM investigation of the bare carbon textile extracted from the cementitious matrix after thermal preconditioning and testing at relatively (a) low and (b) high magnification.


(a)

(b)
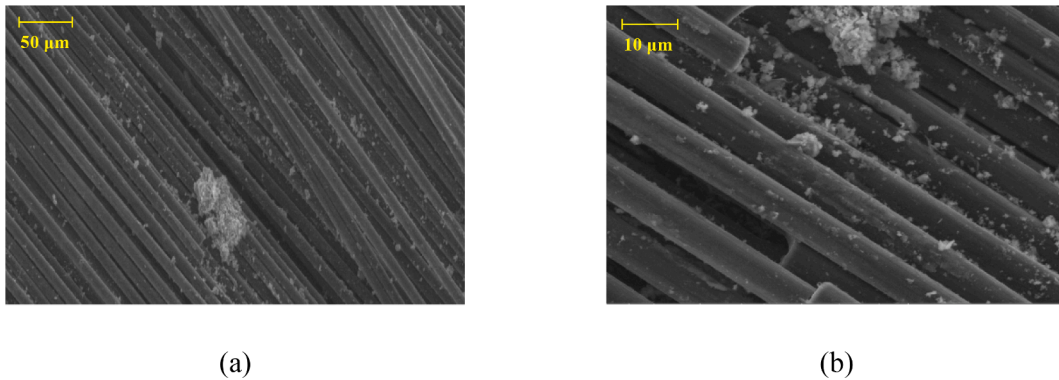
Fig. 16. SEM investigation of impregnated carbon textile extracted from the cementitious matrix after thermal preconditioning and testing at relatively (a) low and (b) high magnification.
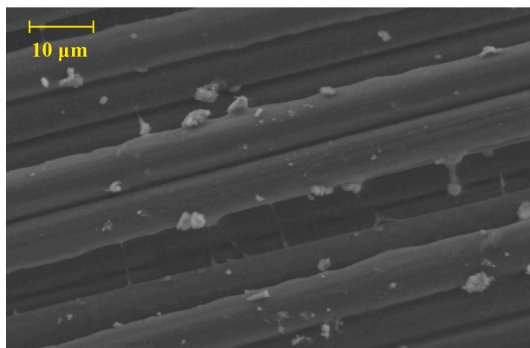
Fig. 17. SEM image showing the coating layer wrapped around the fibers and mortar patches adhered to it.

scattering remained very limited regardless of the enhanced mechanical properties. This leads to important consequences in terms of design values, whereby improved mechanical properties are to be weighed against result consistency. Furthermore, the organic phase greatly improved the exploitation ratio of the textile, in both control and preconditioned specimens.

The results obtained revealed that the inorganic phase was capable of shielding the organic phase from thermal degradation to a large extent. Three main advantages were achieved over the fully inorganic system, namely the performance level, performance consistency, and material optimization/exploitation. Considering these results, it is concluded that engineering an organic phase into an inorganic system may be among the best strategies for inorganic composite improvement.

(a)

(b)
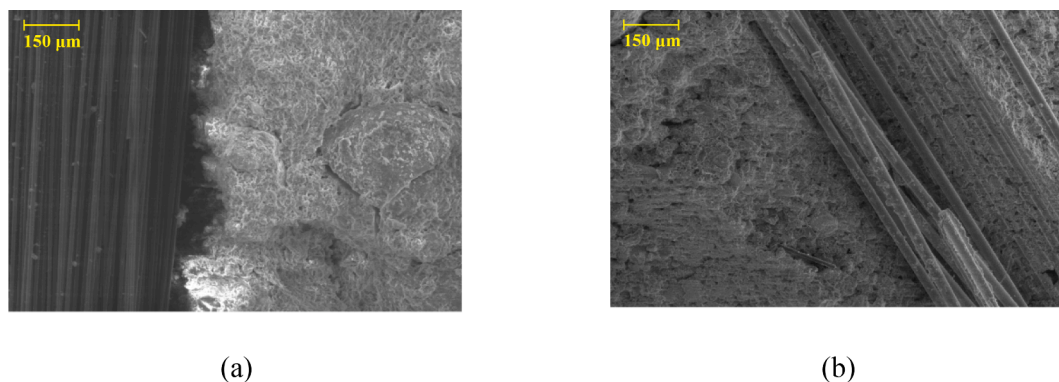
Fig. 18. SEM investigation of failed specimens focusing on the mortar porosity (a) before (i.e., control specimen) and (b) after preconditioning.

CRediT authorship contribution statement

Veronica Bertolli: Writing – original draft, Investigation, Formal analysis. **Cesare Signorini:** Writing – original draft, Investigation, Formal analysis. **Andrea Nobili:** Writing – review & editing, Supervision, Resources, Conceptualization. **Tommaso D'Antino:** Writing – review & editing, Supervision, Resources, Methodology, Conceptualization.

Declaration of Competing Interest

The authors declare that they have no known competing financial interests or personal relationships that could have appeared to influence the work reported in this paper.

Data availability

Data will be made available on request.

References

[1] C.G. Papanicolaou, T.C. Triantafillou, M. Papathanasiou, K. Karlos, Textile reinforced mortar (TRM) versus FRP as strengthening material of URM walls: Out-of-plane cyclic Loading, Mater. Structu./MATERIAux et Constr. 41 (2008) 143–157, https://doi.org/10.1617/s11527-007-9226-0.

[2] G. de Felice, S. De Santis, L. Garmendia, B. Ghiassi, P. Larrinaga, P.B. Lourenço, D. V. Oliveira, F. Paolacci, C.G. Papanicolaou, Mortar-based systems for externally bonded strengthening of masonry, Mater. Struct. 47 (2014) 2021–2037, https://doi.org/10.1617/s11527-014-0360-1.

[3] R. Grazzini, G. Misseri, L. Rovero, A Bi-modulus material model for bending test on NHL3.5 lime mortar, Mater. 16 (2023) 486, https://doi.org/10.3390/ma16020486.

[4] F. Bencardino, C. Carloni, A. Condello, F. Focacci, A. Napoli, R. Realfonzo, Flexural behaviour of RC members strengthened with FRCM: State-of-the-art and predictive formulas, Compos. B. Eng. 148 (2018) 132–148, https://doi.org/10.1016/j.compositesb.2018.04.051.

[5] C. Signorini, A. Nobili, A. Sola, M. Messori, Designing epoxy viscosity for optimal mechanical performance of coated Glass Textile Reinforced Mortar (GTRM) composites, Constr. Build. Mater. 233 (2020) 117325, https://doi.org/10.1016/j.conbuildmat.2019.117325.

[6] M. Rodríguez-Marcos, P. Villanueva-Llaurado, J. Fernández-Gómez, J. López-Rebollo, Improvement of tensile properties of carbon fibre-reinforced cementitious matrix composites with coated textile and enhanced mortars, Constr. Build. Mater. 369 (2023) 130552, https://doi.org/10.1016/j.conbuildmat.2023.130552.

[7] R. Nadiv, A. Peled, V. Mechtcherine, S. Hempel, C. Schroefl, Micro- and nanoparticle mineral coating for enhanced properties of carbon multifilament yarn cement-based composites, Compos. B Eng. 111 (2017) 179–189, https://doi.org/10.1016/j.compositesb.2016.12.005.

[8] B. Mobasher, A. Peled, J. Pahilajani, Distributed cracking and stiffness degradation in fabric-cement composites, Mater. Struct. 39 (2006) 317–331.

[9] F. Bompadre, J. Donnini, Surface Modification of Glass Textile for the Reinforcement of a Cement-Based Composite: A Review, Appl. Sci. 11 (2021) 2028, https://doi.org/10.3390/app11052028.

[10] J. Donnini, V. Corinaldesi, A. Nanni, Mechanical properties of FRCM using carbon fabrics with different coating treatments, Compos. B Eng. 88 (2016) 220–228, https://doi.org/10.1016/j.compositesb.2015.11.012.

[11] M. Messori, A. Nobili, C. Signorini, A. Sola, Mechanical performance of epoxy coated AR-Glass fabric Textile Reinforced Mortar: Influence of coating thickness and formulation, Compos. B. Eng. 149 (2018) 135–143.

[12] D. Arboleda, S. Babaeidarabad, C.D.L. Hays, A. Nanni, Durability of Fabric Reinforced Cementitious Matrix (FRCM) Composites, in: International Institute for FRP in Construction (IIFC), 2014.

[13] F. Micelli, M.A. Aiello, Residual tensile strength of dry and impregnated reinforcement fibres after exposure to alkaline environments, Compos. B Eng. 159 (2017) 490–501, https://doi.org/10.1016/j.compositesb.2017.03.005.

[14] C. Signorini, A. Nobili, F.O. Falope, Mechanical performance and crack pattern analysis of aged carbon fabric cementitious matrix (CFRCM) composites, Compos. Struct. (2018), https://doi.org/10.1016/j.compstruct.2018.05.052.

[15] M. De Munck, M. El Kadi, E. Tsangouri, J. Vervloet, S. Verbruggen, J. Wastiels, T. Tysmans, O. Remy, Influence of environmental loading on the tensile and cracking behaviour of textile reinforced cementitious composites, Constr. Build. Mater. 181 (2018) 325–334, https://doi.org/10.1016/j.conbuildmat.2018.06.045.

[16] J. Donnini, Durability of glass FRCM systems: Effects of different environments on mechanical properties, Compos. B. Eng. (2019) 107047.

[17] International Code Council Evaluation Service (ICC-ES), Acceptance criteria for masonry and concrete strengthening using fabric-reinforced cementitious matrix (FRCM) and steel reinforced grout (SRG) composite systems. AC434, Whittier, CA, 2018. https://icc-es.org/acceptance-criteria/ac434/.

[18] CSLLPP - Servizio Tecnico Centrale, Linee Guida per la identificazione, la qualificazione ed il controllo di accettazione di compositi fibrorinforzati a matrice inorganica (FRCM) da utilizzarsi per il consolidamento strutturale di costruzioni esistenti, Rome, Italy, 2019.

[19] European Organisation for Technical Assessment (EOTA), Externally-bonded composite systems with inorganic matrix for strengthening of concrete and masonry structures. EAD 340275-00-0104, EOTA, Brussels, Belgium, 2018.

[20] C. Signorini, A. Nobili, Comparing durability of steel reinforced grout (SRG) and textile reinforced mortar (TRM) for structural retrofitting, Mater. Struct. 54 (2021) 1–15, https://doi.org/10.1617/s11527-021-01729-3.

[21] P.D. Askouni, C.G. Papanicolaou, M.I. Kaffetzakis, The effect of elevated temperatures on the TRM-to-masonry bond: comparison of normal weight and lightweight matrices, Appl. Sci. 9 (2019) 2156, https://doi.org/10.3390/app9102156.

[22] S.S. Tabatabaei, R. Fayaz, The effect of facade materials and coatings on urban heat island mitigation and outdoor thermal comfort in hot semi-arid climate, Build. Environ. (2023), 110701, https://doi.org/10.1016/j.buildenv.2023.110701.

[23] Ministero delle Infrastrutture e dei Trasporti, Aggiornamento delle Norme Tecniche per le Costruzioni, Gazzetta Ufficiale della Repubblica Italiana, Rome, Italy, 2018.

[24] European Committee for Standardization, EN 1991-1-2 Eurocode 1: Actions on Structures, CEN - European Committee for Standardization, 2002.

[25] BS EN ISO 13943, Fire safety - Vocabulary, 2017.

[26] BS EN 13501, Fire classification of construction products and building elements, 2023.

[27] ACI PRC-549.4-20, Guide to Design and Construction of Externally Bonded Fabric-Reinforced and Steel-Reinforced Grout Systems for Repair and Strengthening of Concrete Structures, American Concrete Institute, 2020.

[28] J. Donnini, F. De Caso y Basalo, V. Corinaldesi, G. Lancioni, A. Nanni, Fabric-reinforced cementitious matrix behavior at high-temperature: Experimental and numerical results, Composites Part B: Engineering. 108 (2017) 108–121. doi: 10.1016/j.compositesb.2016.10.004.

[29] M. Messori, A. Nobili, C. Signorini, A. Sola, Effect of high temperature exposure on epoxy-coated glass textile reinforced mortar (GTRM) composites, Constr. Build. Mater. 212 (2019) 765–774, https://doi.org/10.1016/j.conbuildmat.2019.04.026.

[30] D.A.S. Rambo, F. de Andrade Silva, R.D. Toledo Filho, O. da F.M. Gomes, Effect of elevated temperatures on the mechanical behavior of basalt textile reinforced refractory concrete, Mater. Design. 65 (2015) 24–33.

[31] P. Kapsalis, T. Tysmans, D. Van Hemelrijck, T. Triantafillou, State-of-the-art review on experimental investigations of textile-reinforced concrete exposed to high temperatures, J. Compos. Sci. 5 (2021) 290, https://doi.org/10.3390/jcs5110290.

[32] S.R. Maroudas, C.G. Papanicolaou, Effect of high temperatures on the TRM-to-masonry bond, KEM. 747 (2017) 533–541, https://doi.org/10.4028/www.scientific.net/KEM.747.533.

[33] S.M. Raoof, D.A. Bournas, Bond between TRM versus FRP composites and concrete at high temperatures, Compos. B Eng. 127 (2017) 150–165, https://doi.org/10.1016/j.compositesb.2017.05.064.

[34] L. Ombres, Analysis of the bond between fabric reinforced cementitious mortar ({FRCM}) strengthening systems and concrete, Compos. B Eng. 69 (2015) 418–426.

[35] L. Ombres, A. Iorfida, S. Mazzuca, S. Verre, Bond analysis of thermally conditioned FRCM-masonry joints, Measurement 125 (2018) 509–515, https://doi.org/10.1016/j.measurement.2018.05.021.

[36] L. Estevan, F.J. Baeza, F.B. Varona, J. Pereiro, Effect of high temperature on textile reinforced mortar-to-masonry bond, Constr. Build. Mater. 393 (2023), 132123, https://doi.org/10.1016/j.conbuildmat.2023.132123.

[37] F. Ferretti, M. Canestri, C. Mazzotti, Effect of temperature variations on the bond behavior of FRCM applied to masonry, Mater. Struct. 55 (2022) 166, https://doi.org/10.1617/s11527-022-02002-x.

[38] F. Abu Obaida, T. El-Maaddawy, H. El-Hassan, Bond Behavior of Carbon Fabric-Reinforced Matrix Composites: Geopolymeric Matrix versus Cementitious Mortar, Buildings 11 (2021) 207, https://doi.org/10.3390/buildings11050207.

[39] P.D. Askouni, C.G. Papanicolaou, L. Azdejkovic, Experimental Investigation of the TRM-to-Masonry Bond after Exposure to Elevated Temperatures: Cementitious and Alkali-Activated Matrices of Various Densities, Materials 15 (2021) 140, https://doi.org/10.3390/ma15010140.

[40] Fibrenet S.r.L., Technical datasheet of Betontex FB-RC225-TH12, (2020). https://www.fibrenet.it/wp-content/uploads/2018/05/BETONTEX-FB-03-STC-104-IT-01-FB-RC225-TH12-R8.pdf.

[41] Ruregold S.r.L., Technical datasheet of MX-PBO muratura, (2020). https://www.ruregold.com/it/download-schede-tecniche/.

[42] European Committee for Standardization, Methods of test for mortar for masonry. Part 6: Determination of bulk density of fresh mortar. EN 1015-6:1999, CEN, Brussels, Belgium, 2007.

[43] A.T. DiBenedetto, Prediction of the glass transition temperature of polymers: a model based on the principle of corresponding states, J. Polym. Sci. B 25 (1987) 1949–1969, https://doi.org/10.1002/polb.1987.090250914.

[44] M.J. Marks, R.V. Snelgrove, Effect of Conversion on the Structure−Property Relationships of Amine-Cured Epoxy Thermosets, ACS Appl. Mater. Interfaces 1 (2009) 921–926, https://doi.org/10.1021/am900030u.

[45] C. Signorini, A. Nobili, A. Sola, M. Messori, Optimal epoxy dilution for epoxy-coated textile reinforced mortar (TRM): An experimental perspective, in: Springer, 2020: pp. 499–511. doi: 10.1007/978-3-030-41057-5_41.

[46] European Committee for Standardization, Methods of test for mortar for masonry. Determination of flexural and compressive strength of hardened mortar. EN 1015-11:1999, CEN, Brussels, Belgium, 2019.

[47] Danesi S.r.L., Technical datasheet of Solid Brick 11.6.24, (2020). https://www.danesilaterizi.it/product/mattone-pieno-11-6-24-mattoni-pieni-prezzo/.

[48] Fassa Bortolo S.r.L., Technical datasheet of MS 20, (2020). https://www.fassabortolo.it/documents/10179/536572/FASSA_STE_IT_MS-20_2022-02.pdf/cc9149c0-653d-469c-9d45-0382089046d8.

[49] T. D'Antino, L.H. Sneed, C. Carloni, C. Pellegrino, Effect of the inherent eccentricity in single-lap direct-shear tests of PBO FRCM-concrete joints, Comp Struct. 142 (2016) 117–129, https://doi.org/10.1016/j.compstruct.2016.01.076.

[50] X. Zhang, W. He, Y. Zhang, C. Chen, X. Wu, Tensile Behavior of Basalt-Fiber-Grid-Reinforced Mortar before and after Exposure to Elevated Temperature, Buildings 12 (2022) 2269, https://doi.org/10.3390/buildings12122269.

[51] P. Valeri, M. Fernàndez Ruiz, A. Muttoni, Tensile response of textile reinforced concrete, Constr. Build. Mater. 258 (2020) 119517, https://doi.org/10.1016/j.conbuildmat.2020.119517.

[52] T. D'Antino, C. Poggi, Stress Redistribution in Glass Fibers of G-FRCM Composites, Key Eng. Mater. 817 (2019) 520–527, https://doi.org/10.4028/www.scientific.net/KEM.817.520.

[53] I. Hager, Colour Change in Heated Concrete, Fire Technol. 50 (2014) 945–958, https://doi.org/10.1007/s10694-012-0320-7.

[54] N.R. Short, J.A. Purkiss, S.E. Guise, Assessment of fire damaged concrete using colour image analysis, Constr. Build. Mater. 15 (2001) 9–15, https://doi.org/10.1016/S0950-0618(00)00065-9.

[55] T.Z. Harmathy, Thermal properties of concrete at elevated temperatures, J. Mater. 5 (1970) 47–74.

[56] F.S. Rostásy, R. Weiβ, G. Wiedemann, Changes of pore structure of cement mortars due to temperature, Cem. Concr. Res. 10 (1980) 157–164, https://doi.org/10.1016/0008-8846(80)90072-1.

[57] M. Lion, F. Skoczylas, Z. Lafhaj, M. Sersar, Experimental study on a mortar. Temperature effects on porosity and permeability. Residual properties or direct measurements under temperature, Cem. Concr. Res. 35 (2005) 1937–1942, https://doi.org/10.1016/j.cemconres.2005.02.006.

[58] M. Colombo, M. di Prisco, R. Felicetti, Mechanical properties of steel fibre reinforced concrete exposed at high temperatures, Mater. Struct. 43 (2010) 475–491, https://doi.org/10.1617/s11527-009-9504-0.

[59] A.S. Calabrese, P. Colombi, T. D'Antino, Analytical solution of the bond behavior of FRCM composites using a rigid-softening cohesive material law, Compos. B Eng. 174 (2019), 107051, https://doi.org/10.1016/j.compositesb.2019.107051.

[60] T. D'Antino, C. Carloni, L.H. Sneed, C. Pellegrino, Matrix–fiber bond behavior in PBO FRCM composites: A fracture mechanics approach, Eng. Fract. Mech. 117 (2014) 94–111, https://doi.org/10.1016/j.engfracmech.2014.01.011.

[61] V. Bertolli, T. D'Antino, Modeling the behavior of externally bonded reinforcement using a rigid-trilinear cohesive material law, Int. J. Solids Struct. 248 (2022), 111641, https://doi.org/10.1016/j.ijsolstr.2022.111641.

[62] J. Hartig, U. Häußler-Combe, K. Schicktanz, Influence of bond properties on the tensile behaviour of Textile Reinforced Concrete, Cem. Concr. Compos. 30 (2008) 898–906, https://doi.org/10.1016/j.cemconcomp.2008.08.004.

[63] T. D'Antino, C. Poggi, Characterization and Design of Multilayer PBO FRCM Composite Reinforcements for Concrete Structures, J. Compos. Constr. 25 (2021) 04021048, https://doi.org/10.1061/(ASCE)CC.1943-5614.0001155.

[64] A. Peled, E. Zaguri, G. Marom, Bonding characteristics of multifilament polymer yarns and cement matrices, Compos. A Appl. Manuf. 39 (2008) 930–939, https://doi.org/10.1016/j.compositesa.2008.03.012.

[65] J. Jiang, C. Jiang, B. Li, P. Feng, Bond behavior of basalt textile meshes in ultra-high ductility cementitious composites, Compos. B Eng. 174 (2019), 107022, https://doi.org/10.1016/j.compositesb.2019.107022.

[66] M. Zhu, J.-H. Zhu, T. Ueda, M. Su, F. Xing, A method for evaluating the bond behavior and anchorage length of embedded carbon yarn in the cementitious matrix, Constr. Build. Mater. 255 (2020) 119067, https://doi.org/10.1016/j.conbuildmat.2020.119067.

[67] S.M. Raoof, L.N. Koutas, D.A. Bournas, Bond between textile-reinforced mortar ({TRM}) and concrete substrates: Experimental investigation, Compos. B Eng. 98 (2016) 350–361.

[68] M. Santandrea, F. Focacci, C. Mazzotti, F. Ubertini, C. Carloni, Determination of the interfacial cohesive material law for SRG composites bonded to a masonry substrate, Eng. Fail. Anal. 111 (2020), 104322, https://doi.org/10.1016/j.engfailanal.2019.104322.

[69] M. Leone, M.A. Aiello, A. Balsamo, F.G. Carozzi, F. Ceroni, M. Corradi, M. Gams, E. Garbin, N. Gattesco, P. Krajewski, C. Mazzotti, D. Oliveira, C.G. Papanicolaou, G. Ranocchiai, F. Roscini, D. Saenger, Glass fabric reinforced cementitious matrix: Tensile properties and bond performance on masonry substrate, Compos. B Eng. 127 (2017) 196–214, https://doi.org/10.1016/j.compositesb.2017.06.028.

[70] A.S. Calabrese, T. D'Antino, P. Colombi, C. Poggi, Study of the influence of interface normal stresses on the bond behavior of FRCM composites using direct shear and modified beam tests, Constr. Build. Mater. 262 (2020), https://doi.org/10.1016/j.conbuildmat.2020.120029.

[71] C. Sauder, J. Lamon, R. Pailler, The tensile behavior of carbon fibers at high temperatures up to 2400 °C, Carbon 42 (2004) 715–725, https://doi.org/10.1016/j.carbon.2003.11.020.

[72] J.P. Firmo, J.R. Correia, L.A. Bisby, Fire behaviour of FRP-strengthened reinforced concrete structural elements: A state-of-the-art review, Compos. B Eng. 80 (2015) 198–216, https://doi.org/10.1016/j.compositesb.2015.05.045.

[73] R.M. de C. Silva, J. Zhao, M. Liebscher, I. Curosu, F. de A. Silva, V. Mechtcherine, Bond behavior of polymer- and mineral-impregnated carbon fiber yarns towards concrete matrices at elevated temperature levels, Cement and Concrete Composites. 133 (2022) 104685. doi: 10.1016/j.cemconcomp.2022.104685.